THE JOURNAL OF BIOLOGICAL CHEMISTRY
Vol. 279, No. 10, Issue of March 5, pp. 9522–9531, 2004
Printed in U.S.A.

Dissecting the EphA3/Ephrin-A5 Interactions Using a Novel Functional Mutagenesis Screen*

Received for publication, August 22, 2003, and in revised form, November 19, 2003
Published, JBC Papers in Press, December 2, 2003, DOI 10.1074/jbc.M309326200

Fiona M. Smith‡§, Christopher Vearing§¶, Martin Lackmann§¶§§, Herbert Treutlein‖, Juha Himanen, Ke Chen‡, Allan Saul‡, Dimitar Nikolov**, and Andrew W. Boyd‡ ‡‡**

*From the ‡Leukaemia Foundation of Queensland Laboratory, Queensland Institute of Medical Research, P. O. Royal Brisbane Hospital, Queensland 4029, ¶Ludwig Institute for Cancer Research (Melbourne Branch), P. O. Royal Melbourne Hospital, Victoria 3050, ‖Cytopia, Baker Heart Research Institute Building, Commercial Road, Melbourne 3004, Australia, **Cellular Biochemistry and Biophysics Program, Memorial Sloan Kettering Cancer Center, New York, New York 11973, and the ‡‡Department of Medicine, University of Queensland, P. O. Royal Brisbane Hospital, Queensland 4029, Australia*

The EphA3 receptor tyrosine kinase preferentially binds ephrin-A5, a member of the corresponding subfamily of membrane-associated ligands. Their interaction regulates critical cell communication functions in normal development and may play a role in neoplasia. Here we describe a random mutagenesis approach, which we employed to study the molecular determinants of the EphA3/ephrin-A5 recognition. Selection and functional characterization of EphA3 point mutants with impaired ephrin-A5 binding from a yeast expression library defined three EphA3 surface areas that are essential for the EphA3/ephrin-A5 interaction. Two of these map to regions identified previously in the crystal structure of the homologous EphB2-ephrin-B2 complex as potential ligand/receptor interfaces. In addition, we identify a third EphA3/ephrin-A5 interface that falls outside the structurally characterized interaction domains. Functional analysis of EphA3 mutants reveals that all three Eph/ephrin contact areas are essential for the assembly of signaling-competent, oligomeric receptor-ligand complexes.

Eph receptor tyrosine kinases (Ephs)[1] are activated through interaction with cell surface-bound ephrin proteins. Binding preferences and structural features classify eight type A Ephs interacting with six type A ephrins that attach to the membrane via glycophosphatidylinositol, as well as six type B Ephs interacting with corresponding type B transmembrane ephrins, which contain conserved cytoplasmic domains (1). Eph/ephrin contacts on opposing cells direct cell movements underlying developmental patterning events (2, 3) but may also regulate tumor cell positioning during cancer metastasis and invasion (4). In many cases Eph signaling results in cytoskeletal collapse, down-regulation of cell-cell adhesion proteins, and cell rounding (2, 5). Concurrent protease-mediated cleavage of the Eph/ephrin linkages (6) leads to cell-cell detachment and repulsion. Interestingly, Eph/ephrin interactions can also promote cell adhesion, a dichotomy of function that has been widely recognized (2, 7, 8).

Ephs have a highly conserved domain structure throughout the animal kingdom (9). The extracellular domain (ECD) consists of a unique N-terminal globular structure, necessary and sufficient for ephrin binding (10, 11), followed by a cysteine-rich linker, an EGF-like motif, and two type II fibronectin domains. For human EphA3 (12), these regions span amino acid sequence positions 29–203, 204–260, 271–324, 325–435, and 435–531, respectively. The minimal N-terminal globular domain has a β jellyroll-like architecture (13), whereas structures of the cysteine-rich linker and adjoining EGF motif have not been solved to date.

Clearly, all Eph/ephrin signaling is initiated by a 1:1 interaction between the globular Eph domain and a conserved Eph-binding domain of the ephrins (14). Furthermore, functional studies have indicated that biological responses rely on oligomerized ephrins to assemble active Eph receptor clusters capable of triggering downstream signaling cascades (15, 16). In agreement, the x-ray crystal structure of the complexed EphB2 and ephrin-B2 interaction domains (17) reveals a 2:2 heterotetramer, containing two types of ligand-receptor contacts of apparent higher affinity (mediating heterodimerization) and lower affinity (mediating heterotetramerization). This configuration of Eph and ephrin domains, where ephrin and Eph C termini are positioned on opposite sites of a ring-like planar structure, illustrates how membrane-associated ephrins and Eph receptors can initiate bi-directional signaling between adjacent cells (18). However, to date there has been little functional data to validate the Eph/ephrin interaction model proposed in the crystal structure. In addition, the possible contributions of other Eph domains to the active signaling complex have not been addressed. Interestingly, earlier *in vivo* studies indicate a requirement of direct Eph-Eph interaction via the cysteine-rich motif for Eph function during early development (11, 17). Although the underlying ephrin-independent Eph dimerization can trigger trans-phosphorylation *in vitro*, it is clear that ephrin-dependent and -independent Eph activation result in distinct downstream signaling and biological response pathways (5).

To examine the mechanism of ephrin-A5-induced Eph activation in more detail, we generated an expression library of EphA3 ECD point mutants that were selected for proteins of correct conformation with reduced ephrin-A5 binding. We found that some 80% of the 50 identified mutants locate to

* This work was supported by the Leukaemia Foundation of Queensland, the Anti-Cancer Council of Victoria, the Human Frontiers Science Program, and the National Health and Medical Research Council of Australia. The costs of publication of this article were defrayed in part by the payment of page charges. This article must therefore be hereby marked "*advertisement*" in accordance with 18 U.S.C. Section 1734 solely to indicate this fact.

§ These authors contributed equally to this work and should be considered as joint first authors.

§§ To whom correspondence should be addressed: Dept. of Biochemistry and Molecular Biology, Monash University, Clayton, Victoria 3800, Australia. Tel.: 61 3 99 05 37 38; Fax: 61 3 99 05 37 26; E-mail: Martin.Lackmann@med.monash.edu.au.

[1] The abbreviations used are: Ephs, ephrin receptor tyrosine kinases; ECD, extracellular domain; EGF, epidermal growth factor; mAb, monoclonal antibody; w/t, wild type; GFP, green fluorescent protein.

EphA3 regions predicted by the EphB2/ephrin-B2 structure to form part of the Eph/ephrin dimerization and tetramerization interfaces. Furthermore, kinetic analysis and functional assessment of mutant cell surface-expressed, full-length EphA3 validates the requirement of each of these Eph/ephrin contacts for the formation of high affinity, biologically relevant EphA3-ephrin-A5 complexes. Importantly, a distinct third group of mutants, defining a third Eph/ephrin interface, is positioned outside the crystallographically characterized ligand-binding domain, within the cysteine-rich linker previously implicated in receptor/receptor contacts. Although their kinetics analysis indicates only moderate effects on ephrin binding, a matching point mutation in the linker region of cell surface-expressed EphA3 abrogates ephrin-induced phosphorylation and Crk recruitment, emphasizing the functional importance of this interface. This mutagenesis analysis provides, for the first time, functional evidence for the essential contribution of several distinct Eph/ephrin interfaces for the formation of signaling-competent Eph/ephrin hetero-oligomers.

TABLE I
The effect of divalent cations on PCR mutations in the EphA3 template

PCR mix	$MnCl_2$	$MgCl_2$	Total bases sequenced	Mutation rate
	mM			
A	0	7.0	4440	1:370
B	0.1	7.0	4840	1:345
C	0.25	7.0	6600	1:194
D	0.5	7.0	5566	1:118
E	0	1.5	7380	1:1476

TABLE II
Characteristics of the EphA3 mutant yeast expression library

Approximately 2% of all colonies were estimated to be FLAG-negative, hence only 94/108 are informative (shown by an asterisk). Replica filters were screened as described under "Experimental Procedures."

Myc epitope present	IIIA4 binding	ephrin A5 Fc binding	No. colonies	% colonies
+	+	−	45	7
+	−	−	204	30
+	−	+	26	4
+	+	+	308	45
−	−	−	108	16*

EXPERIMENTAL PROCEDURES

Expression Constructs and Reagents

EphA3 and Ephrin-A5 Fc Constructs—A cDNA encompassing bp 103–1692 from full-length human EphA3 (12) was cloned into pIgBOS for expression of the EphA3 exodomain fused to the human IgG1 hinge and Fc regions (EphA3-Fc), as described (19). EphA3-Fc and ephrin-A5 Fc (gift of Dr. D. Cerretti, Immunex Corp., Seattle, WA) were used for stable transfection of Chinese hamster ovary cells. Fc fusion proteins were purified from cell culture supernatants (RPMI 1640, 2.5% immunoglobulin-depleted fetal bovine serum) by protein-A-Sepharose (Amersham Biosciences) affinity chromatography, followed by size-exclusion high pressure liquid chromatography.

Yeast EphA3 Expression Construct—A cDNA encoding the EphA3 extracellular domain (Glu^{21} to Ser^{539}, ECD) was cloned into the yeast expression vector YEpFLAG-1 (Sigma), containing a FLAG epitope and the alcohol dehydrogenase promoter for activation of transcription/translation under low glucose conditions. In addition to a C-terminal *myc* epitope (EEQKLISEEDL*), EcoRI and BglII cloning sites were introduced between the FLAG and Myc sequences to accommodate insertion of EphA3-ECD cDNAs. Accordingly, the 5′-EphA3 oligonucleotide (^{21}ELIPQPSNE^{30}V (12)) was altered to introduce a unique

TABLE III
Yeast mutants isolated by expression screening

[a]AA position	Mutant first	Mutant second	[b]2nd structure
29	E->G		Aβ
37 δ	T->P		A-C
50	H->Q	S_{108}->G*	C-D
53 δ	E->K	D_{59}->G	Dβ
53 δ	E->K	N_{85}->T	Dβ
58 δ	V->A	T_{84}->A	D-E
59 δ	D->V*		D-E
59 δ	D->G	E_{53}->K	D-E
60 δ	E->D		D-E
60 δ	E->V	I_{95}->V	D-E
68 δ	Y->N		Eβ
75(τ)	D->V*		E-F
79	N->T		E-F
84	T->A	V_{58}->A	Fβ
85	N->S	P_{108}->Q	Fβ
85	N->T	E_{53}->K	Fβ
91 τ	S->P*		F-G
95	I->V	E_{60}->V	Gβ
102 δ	T->A	K_{200}->I	Gβ
105 δ	D->E	I_{168}->N	G-H
108 δ	S->G	H_{50}->Q	G-H
109 δ	I->T		G-H
110 δ	P->Q		G-H
110 δ	P->Q	N_{85}->S	G-H
111 δ	L->F		G-H

[a]AA position	Mutant first	Mutant second	Mutant third	[b]2nd structure
130 τ	D->G*			H-I
130 τ	D->G*			H-I
132 τ	G->E*			H-I
133 τ	V->E	R_{136}->P		H-I
136 τ	R->P	V_{133}->E		H-I
140	F->L			H-I
150 δ	E->G	Y_{278}->N		Jβ
151 δ	S->G	M_{218}->K		Jβ
152 δ	F->L*			Jβ
165(τ)	N->Y	N_{232}->I		Kβ
168	I->N	D_{105}->E		Kβ
177 τ	K->R			K-L
189 δ	C->F			L-M
200	K->E			Mβ
200	K->I	T_{102}->A		Mβ
208 γ	N->K			
209 γ	L->Q	M_{218}->I*		
218 γ	M->I	L_{209}->Q		
218 γ	M->K	S_{151}->G		
231 γ	V->D	A_{272}->V	L_{281}->W*	
232 γ	N->I	N_{165}->Y		
233 γ	N->S			
245 γ	S->R			
259 γ	C->R			
272 γ	A->V			
281 γ	L->W			

[a] Amino acid (AA) residue numbers are in accord with the published sequence (12). The symbols δ and τ indicate that this site is homologous to a residue in EphB2, which forms part of the dimerization and tetramerization interfaces, respectively. For double and triple mutant clones (*i.e.* containing two or three mutated residues), the second listed positions are highlighted by shading.

[b] Secondary (2nd) structure elements are assigned according to the EphB2/ephrin-B2 structure (17) (β; β-sheet).

* These mutants showed weak or marginal IIIA4 antibody binding.

γ These residues lie C-terminal to the EphB structure characterized by crystallography (17).

TABLE IV
Binding characteristics of EphA3 mutants to an ephrin-A5 sensor surface

γ indicates mutants designed by alignment with EphB2/ephrin-B2 structure. * indicates not done (n.d.), lack of IIIA4 binding hindered purification of assayable protein.

		Ephrin-A5			IIIA4
[a]Binding site	Mutation	[b]k_a(1/Ms) x 10^5	[b]k_d(1/s)	[b]K_D(nM)	[b]K_D(nM)
	sEphA3	1.62	0.014	86	5.9
	w/t	1.230	0.008	58	3.1
δ	¥41E->R	0.214	0.0291	1360	3.9
δ	50 H->Q	0.0791	0.0131	1650	37.2
δ	53 E ->K	ephrin binding below range (k_a~202)			15.6
δ	58V->A	0.0421	0.0197	4680	9.9
δ	68Y->N	0.695	0.0228	328	9.5
δ	75D->V	0.348	0.0123	354	8.0
	85 N->T	1.02	0.0126	124	5.3
δ	102T->A	ephrin binding below range (k_a~100)			9.4
δ	¥102T->Q	ephrin binding below range (k_a<100)			10.0
δ	¥104R->E	ephrin binding below range (k_a~360)			5.9
δ	108S->G	0.475	0.078	1660	7.6
δ	109I->T	ephrin binding below range (k_a~846)			27.4
δ	111L->F	0.882	0.124	141	15.2
	150E->G	ephrin binding below range (k_a~38)			15.1
	151 S-> G	0.515	0.0938	1820	15.2
	152F->L	ephrin binding below range (k_a<10)			15.0
	165N->Y	0.0296	0.005	1,650	13.6
τ	91S->P	1.67	0.0145	86.9	7.0
τ	*130D->G	n.d.	n.d.	n.d.	n.d.
τ	132G->E	0.031	0.009	2811	1480
τ	133V->E	0.401	0.012	311	579
τ	200 K->I	0.432	0.0139	323	18.7
γ	208N->K	0.242	0.0115	476	661
γ	209L->Q	2.14	0.0216	101	11.4
γ	218M->K	0.448	0.0133	298	16
γ	218M->I	0.414	0.012	290	16
γ	*231V->D	n.d.	n.d.	n.d.	n.d.
γ	232N->I	0.520	0.0232	446	15
γ	245S-> R	1.25	0.0178	142	7.4

[a] Position of mutants assigned by alignment with EphB2/ephrin-B2 structure.

[b] Kinetic properties of mutant proteins binding BIAcore SensorChip-bound ephrin-A5 or IIIA4 mAb were determined by global analysis using BIAevaluation software (version 3.2) as described previously (24).

δ indicates amino acid positions corresponding to the EphB2/ephrin-B2 dimerization interface.

τ indicates amino acid positions corresponding to the EphB2/ephrin-B2 tetramerization interface.

γ indicates amino acid positions outside the EphB2/ephrin-B2 crystal structure (17).

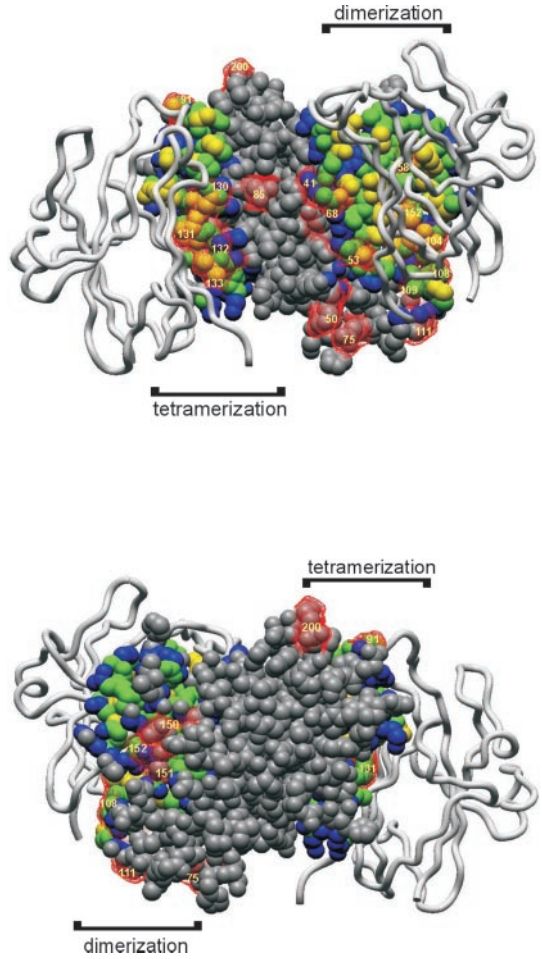

FIG. 1. **Putative molecular model of the complex between the EphA3 globular domain and ephrin-A5.** The atomic coordinates of the EphB2/ephrin-B2 crystal structure (17) were used to assemble a model structure of the corresponding EphA3 and ephrin-A5 domains using MODELLER (version 6) and InsightII software. The model illustrates the putative Eph/ephrin dimerization and heterotetramerization interfaces occupied by ephrin-A5 molecules. For reasons of clarity the second EphA3 ligand-binding domain of the tetrameric complex is omitted. The *bottom panel* represents a 180° rotated view of the complex. The carbon backbone of ephrin-A5 molecules is displayed as tube diagram and the EphA3 ligand-binding domain represented as space-filling atomic model. EphA3 residues are color-coded according to their predicted proximity to Eph/ephrin interaction sites: *yellow* (4 Å), *green* (6 Å), *blue* (8 Å), and *gray* (>8 Å). Altered residues of EphA3 mutants that have been analyzed by kinetic BIAcore analysis (Table IV) are marked by *red shading* and also by their corresponding amino acid position within the EphA3 sequence.

EcoRI site (Leu[22], CTG to Phe, TTC) at the junction of FLAG and EphA3 sequences, and a BglII sequence was added to the 3′-oligonucleotide (corresponding to [534]SISGES). A unique BamHI site was further created by a silent mutation at nucleotides 997–1002 within the exon IV-encoded EGF-like domain. The EphA3 protein derived from this construct was detectable with either anti-FLAG antibody (M2, Sigma) or the anti-Myc antibody (9E10, generous gift from Dr. D. Huang, The Walter and Eliza Hall Institute for Medical Research) and bound ephrin-A5 with comparable affinity to the wild-type receptor.

Random Mutagenesis

Mutants of the EphA3 ECD were created by random mutagenesis using non-stringent PCR (20). Conditions were optimized to yield 3–4 mutations or 1–3 amino acid changes per clone, so that 500 independent clones with some 1000 mutated amino acid residues provided a 4-fold mutational coverage of the target sequence (Table I).

The EcoRI- and BamHI-digested PCR products were ligated into the EphA3-YEpFLAG-1 vector and the resulting mutant plasmid library, encoding EphA3 ECD with mutations in the ligand-binding domain and cysteine-rich linker, and the N-terminal half of the EGF-like domain (Ala[272] to Ser[301]) was amplified in *Escherichia coli*. Plasmid cDNAs from pooled colonies (~13,000) were transfected into the *Saccharomyces cerevisiae* strain BJ3505 containing the plasmid TRP1 gene for selection in tryptophan-deficient media (SD growth medium). Individual colonies were seeded into parallel 96-well trays containing selection medium or normal agar culture medium covered with cellulose nitrate filters. EphA3 protein expression in colonies was induced by transfer of the cellulose filters to zero glucose YPEM medium, and secreted proteins were captured by absorption onto 3–4 replicate nitrocellulose filters for screening. Individual filters from each set of replicates were probed with monoclonal antibodies (mAbs) against EphA3 (IIIA4), the Myc epitope (9E10), the FLAG epitope (M2), and with ephrinA5-Fc. Horseradish peroxidase-conjugated secondary antibodies (Dako) were used for detection. Colonies showing reduced ephrin-A5 binding were recovered, and DNA was extracted for sequence analysis of the EphA3 (EcoRI-BamHI) inserts.

Site-directed Mutagenesis and Transient Protein Expression

To deconvolute critical EphA3 ECD clones containing more that one amino acid change, individual residues were replicated in the pEF BOS-FLAG-EphA3 mammalian expression vector (11, 14) by site-directed mutagenesis (QuickChange Mutagenesis Kit, Stratagene). Upon DNA sequence confirmation, mutant and wild-type (w/t) EphA3-pEF BOS plasmid DNA was transfected into HEK 293T cells (FuGENE 6, Roche Applied Science), and culture supernatants were harvested after 72 h. EphA3 ECD expression was assessed by Western blot (rabbit anti-EphA3 antibody (14)) and BIAcore analysis using sensor chips

containing ephrin-A5 and IIIA4 on parallel flow channels. All proteins used for kinetic analysis were purified by IIIA4 affinity chromatography (21). The proteins were analyzed by SDS-PAGE/silver staining and Western blot using α-EphA3 (polyclonal) or α-FLAG (monoclonal) antibodies. Western blots were developed using ECL detection (SuperSignal Chemiluminescence, Pierce).

BIAcore Analysis

Purified EphA3 ECD proteins in BIAcore buffer (10 mM Hepes, pH 7.4, 0.15 M NaCl, 3.4 mM EDTA, 0.005% Tween 20) were analyzed at 27 °C on parallel IIIA4 and ephrinA5-derivatized CM5 sensor chips (BIAcore 2000 optical biosensor, BIAcore AB, Sweden). The protein concentrations were determined at A_{215} (21). To ascertain the performance of sensor chip-immobilized proteins, samples of purified EphA3 ECD (62.5–1000 ng/ml) were analyzed in each assay. Interaction kinetics was evaluated from eight serial dilutions of each sample by Global Analysis using the BIAevaluation software (version 3.1).

Alexa Fluor™ 546 EphrinA5-Fc Conjugate and Confocal Microscopy

Purified ephrinA5-Fc was labeled using an Alexa Fluor™ 546 fluorescent labeling kit (Molecular Probes). Coupling of the ALEXA dye and its effect on the biological integrity of ephrin was monitored during the labeling reaction by spectral (high pressure liquid chromatography diode array detection) and BIAcore analysis, respectively. Labeling reactions were terminated when the first decrease in binding was detected. Ephrin binding *in situ* to cells transiently transfected with mutant EphA3-GFP receptors was analyzed by 10 min of incubation with 1.5 μg/ml, human IgG pre-clustered Alexa 546 ephrinA5-Fc. The cells were washed with ice-cold phosphate-buffered saline, fixed using 4% paraformaldehyde, and mounted in distyrene/plasticiser/xylene. Confocal fluorescence microscopy using an Olympus FV500 with an oil immersion objective provided the resulting images.

Modeling of EphA3 Structure

A three-dimensional model of the human EphA3 ligand-binding domain complexed to ephrin-A5 was based on the x-ray crystal coordinates of the corresponding mouse EphB2-ephrin-B2 complex (17), (Protein Data Bank code 1KGY). The human EphA3 sequence and the published sequence alignment (17) (identical EphB2/EphA3 residues are indicated with ".") are as follows:

```
hEphA3:EVNLLDSKTIQGELGWISYPSHGWEEISGVDEHYTPIRTYQVCNVMDHS
mEphB2:.ET.M..T.ATA....MVH.PS....V..Y..NMNT.........FES.
hEphA3:QNNWLRTNWVPRNSAQKIYVELKFTLRDCNSIPLVLGTCKETFNLYYME
mEphB2:.......KFIR.RG.HR.H..M..SV...S...S.P.S.........Y.
hEphA3:SDDDHGVK----FREHQFTKIDTIAADESFTQMDLGDRILKLNTEIREV
mEphB2:A.F.LAT.TFPNWM.NPWV.V.........S.V...G.VM.I...V.SF
hEphA3:GPVNKKGFYLAFQDVGACVALVSVRVYFK
mEphB2:...SRN........Y.G.MS.IA...FYR

mEphrinB2:---IVLEPIYWNSSNSKFLPGGGLVLYPQIGDKLDIICPKVDSKT-VGQY
hEphrinA3:KAVADRYAV......PR.QR-.DYHIDVC.N.Y..VF..HYEDSVPEDKT
mEphrinB2:EYYKVYMVDKDQADRCTIKKENTPLLNCARPDQ---DVKFTIKFQEFSPN
hEphrinA3:.R.VL...NF.GYSA.DHTSKGFKRWE.N..HSPNGPL..SE...LFTPF
mEphrinB2:LWGLEFQKNKDYYIISTSNGSLEGLDNQEGGVCQTRAMKILMKVG-
hEphrinA3:SL.F..RPGRE.FY..SAIPDNGRRS------CLKLKVFVRPTNSC
```

These were used to create 200 models of the ephrin-A5 complexed EphA3 ligand-binding domain using MODELLER (release 6) (22) (Accelrys, San Diego). The models were evaluated for structural quality and compatibility with known protein structures as described (23) using the "ProStat" and "Profiles3D" modules of InsightII (Accelrys, San Diego).

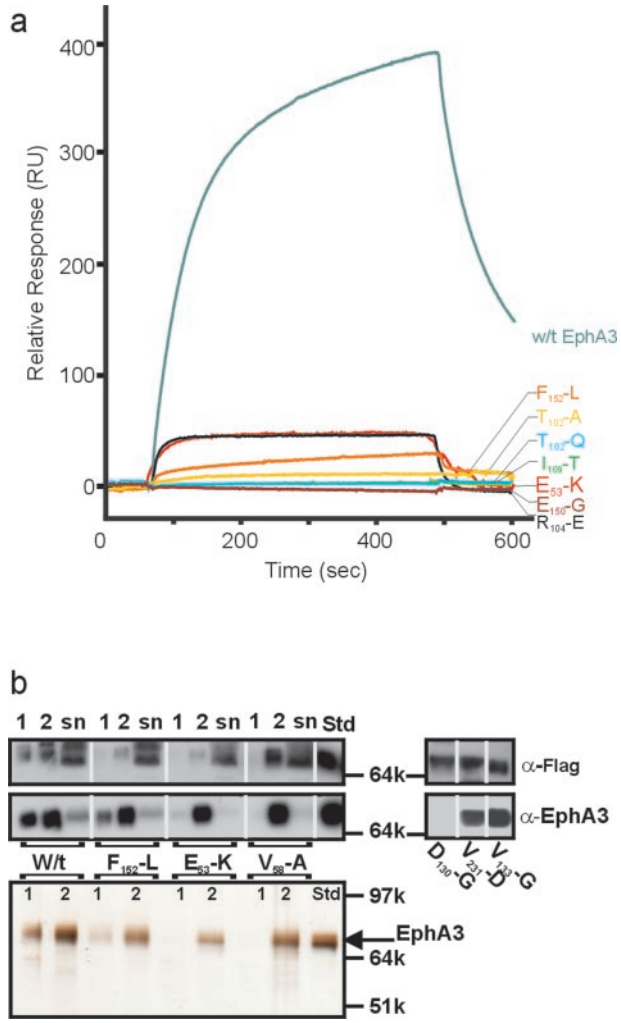

FIG. 2. **Ephrin-A5 binding properties of soluble EphA3 and derived point mutants.** *a*, the binding curves of non-mutated EphA3 extracellular domain (w/t EphA3) and derived point mutants as indicated by amino acid position are illustrated. Binding of the purified proteins was examined (Table IV) by applying serially diluted EphA3 proteins to monovalent ephrin-A5 and a non-relevant control protein (insulin) immobilized on parallel channels of the BIAcore sensor chip surface. The illustrated relative response units (*RU*) represent binding data of EphA3 protein samples at 30 nM that were corrected for sample-related bulk refractive index changes by subtraction of responses monitored on the control surface. *b*, assessment of protein integrity and purity of mutant EphA3 by Western blot and silver staining. The soluble, non-mutated EphA3 extracellular domain (*w/t*) or selected mutants, as indicated, were affinity-purified from cell culture supernatants (*sn*). The affinity column eluates (*lanes 1* and *2*) together with crude supernatants, including those lacking IIIA4 immunoreactivity (D130G, V231D, and V133G), and purified soluble EphA3 (14) were analyzed by anti-FLAG and anti-EphA3 Western blots. Samples from the affinity column eluates were analyzed by silver staining (*bottom panel*). This figure illustrates the analysis for only a small selection of mutant proteins as representative examples.

RESULTS

Library of EphA3 Variants Deficient in EphrinA5 Binding—Our mutagenesis approach targeted an 830-bp EphA3 cDNA fragment spanning the globular ligand binding, the cysteine-rich linker, and the N-terminal part of the EGF-like domain. During optimization we confirmed by sequence analysis of randomly selected bacterial colonies the following: (a) all 4 bases were mutated with similar frequencies; (*b*) there was no apparent restriction in nucleotide placement; and (*c*) mutants were randomly distributed across the entire sequence. This strategy yielded 1300 bacterial YEpFLAG-1 colonies and a derived expression library of ~700 mutant yeast clones. As early results indicated less than 2% of FLAG-negative clones (empty vector or lack of secretion), routine screening for the FLAG epitope was discontinued to preserve samples. The analysis of 677 informative colonies suggests that 50% of the clones produced proteins with apparent defects in ephrin-A5 binding (Table II). To evaluate whether any mutations disrupt the overall protein fold, we used the IIIA4 anti-EphA3 mAb that has been used previously to monitor the EphA3 conformation (21). This mAb binds only to the properly folded N-terminal globular domain of the receptor (11). The 14% Myc-negative mutants were excluded from further analyses as they likely represent prematurely terminated translation products. Of the remaining col-

TABLE V
Binding of ephrin-A5 or ephrin-B2 to sensor surfaces containing EphA3(Val^{133} → Glu), EphA3(Phe^{152} → Leu) and EphA3 (Val^{133}, Phe^{152}) mutants

Analyzed ephrin protein[a]	Immobilized EphA3 protein[b]	k_a[c]	k_d[c]	K_D[c]
		1/ms	*1/s*	*nM*
EphrinA5	w/t	6.2×10^5	0.006	9.6
	Val^{133} → Glu	7.9×10^5	0.02	25.8
	Phe^{152} → Leu	2.4×10^5	0.26	1070
	Val^{133}, Phe^{152}	1.5×10^5	0.229	1580
EphrinB2	w/t		Below BIAcore range	
	Val^{133} → Glu		Below BIAcore range	
	Phe^{152} → Leu		Below BIAcore range	
	Val^{133}, Phe^{152}		Below BIAcore range	
EphrinA5-Fc	w/t	3.4×10^5	4.0×10^{-5}	0.1
	Val^{133} → Glu	4.3×10^5	3.0×10^{-4}	0.7
	Phe^{152} → Leu	3.8×10^5	0.002	5.6
	Val^{133}, Phe^{152}	3.7×10^5	0.003	7.4
EphrinB2-Fc	w/t	1.0×10^4	0.00026	27.1
	Val^{133} → Glu	4.2×10^4	0.0016	35
	Phe^{152} → Leu	7.4×10^4	0.00306	41.2
	Val^{133}, Phe^{152}	3.2×10^4	0.00174	54.2

[a] Soluble ephrins or ephrin-Fc fusion proteins were produced and purified as described previously (14, 17). Serial dilutions between 1 μM and 7.8 nM (monovalent ephrin) and 24 and 0.19 nM (divalent ephrin) were injected across parallel SensorChip surfaces as described under "Experimental Procedures."
[b] Points mutations of EphA3 dimerization and tetramerization domains were introduced into the pIG-EphA3 expression vector by site-directed mutagenesis. Resultant w/t and mutant proteins, purified to homogeneity were immobilized onto parallel channels of BIAcore sensorchips for analysis of ephrin binding.
[c] Kinetic characteristics of BIAcore SensorChip-bound, w/t, and mutant EphA3 Fc binding soluble ephrin were determined by global analysis using BIAevaluation software (version 3.2) as described previously (24).

onies, 334 (57%) retained ephrin-A5 binding, only 26 of which lost immunoreactivity to IIIA4. The majority (79%) of mutants that failed to bind ephrin-A5 also did not bind IIIA4. Only 7% of all mutants lost ephrin-A5 binding capacity while retaining IIIA4 reactivity and were selected for further detailed analysis.

Sequence Analysis Reveals Three Distinct Mutant Clusters Depicting EphA3/Ephrin-A5 Interaction Sites—cDNAs from 38 of the 45 EphA3 clones with compromised ephrin-A5 binding were recovered for sequence analysis. Although the selection of mutants focused on clones binding IIIA4 (Table II), some of these were found to exhibit substantially reduced or marginal IIIA4 reactivity in subsequent assays (indicated by *, Table III, see also Table IV). In a single case, a clone initially negative for ephrin-A5 binding revealed w/t binding characteristics in subsequent assays (Glu^{60} → Asp). In total, sequence analysis revealed 51 single amino acid substitutions in the 38 clones, accounting for the incidence of double (16) and triple mutations (1) in several clones (Table III). These mutants are listed in the context of secondary structure elements of the corresponding EphB2 crystal structure, and their position within the EphB2/ephrin-B2 heterodimerization (δ) or heterotetramerization (τ) interfaces (17) is indicated. As expected, the majority of these (40/51) affects residues that fall within the ligand-binding domain (residues 29–207), and 72.5% (29/40) of these involve residues that are involved in receptor/ligand contacts in the EphB2/ephrin-B2 crystal structure (17). It should be noted that EphA3 residues 150–152 do not have direct EphB2 counterparts but that inspection of the crystal structure reveals their position in the back of the ligand-binding channel (see Fig. 1). Importantly, 8 EphA3 mutants with reduced ephrin-A5 binding capacity map to the cysteine-rich linker region of EphA3 (11), which falls outside the ephrin-binding domain elucidated in the corresponding EphB2 crystal structure (17).

Homology Model of the EphA3-Ephrin-A5 Complex—Based on significant sequence identities between EphB2 and EphA3 ligand-binding domains (56% identity) and between ephrin-B2 and ephrin-A5 receptor-binding domains (~30% identity), we modeled a putative EphA3-ephrin-A5 complex by using the coordinates of the EphB2/ephrin-B2 crystal structure as basis (Fig. 1). The proximity of critical EphA3 residues identified by mutagenesis to the bound ephrin is indicated by *yellow* (4 Å), *green* (6 Å), and *blue* (8 Å) coloring, respectively. The positions of the ephrin-A5-binding mutants within this three-dimensional model (indicated by *red transparent shading* and *yellow numbering*) are concentrated around regions of receptor-ligand contact. Two spatially distinct mutant clusters broadly mirror the ligand-interaction interfaces defined in the EphB2/ephrin-B2 crystal structure (17). Most mutants are in residues belonging to the high affinity dimerization interface, including the B-C and C-D loops (Table III, His^{50} → Gln and Glu^{53} → Lys), the D and E strands (Table III, Val^{58} → Ala and Asp^{75} → Val), the ligand binding groove (Table III, Thr^{102} → Ala and Phe^{152} → Leu), its base (Table IV, Glu^{150} → Gly and Ser^{151} → Gly), and the G-H loop forming the "lid" of the groove (Table III, Ser^{108} → Gly, Ile^{109} → Thr, and Leu^{111} → Phe). Several mutants fall within the Eph/ephrin heterotetramerization interface (Table III, Ser^{91} → Ala, Gly^{132} → Glu, Val^{133} → Glu, and Lys^{200} → Ile), confirming the validity of the tetrameric Eph/ephrin model. In addition to the mutants within the crystallographically characterized domains, three others, which also affected ligand binding (Asn^{208} → Lys, Met^{218} → Lys, and Asn^{232} → Ile), map to the cysteine-rich linker region that connects onto the EGF-like putative receptor-receptor dimerization domain (11).

Kinetic Binding Analysis Distinguishes Three EphA3/Ephrin-A5 Contact Surfaces—From the 51 identified amino acid substitutions, a representative group of 26 mutants contained within or on the back of protein domains with predicted ephrin contacts (Fig. 1), as well as mutants outside the domains described in the model structure, were selected for preparation of mutant EphA3 cDNA for transient expression in HEK 293 cells (Table IV). Although 24 of these yielded proteins suitable for IIIA4 affinity isolation and ephrin-A5 binding analysis by surface plasmon resonance (Fig. 2 and Table IV), two of the listed amino acid substitutions disrupted IIIA4 binding and hindered affinity isolation (Table IV, not done). In addition, three EphA3 point mutants, assigned through alignment to matching EphB2/ephrin-B2 contact surfaces (indicated by ¥ in Table IV) were examined in parallel.

We examined the kinetic properties of mutant, in comparison

to w/t EphA3 ECD proteins, by estimating apparent binding affinities to ephrin-A5 from association and dissociation rate constants, observed in a series of parallel BIAcore experiments. In agreement with earlier studies, Chinese hamster ovary cell-derived FLAG-tagged w/t EphA3, bound sensor chip-coupled ephrin-A5 with comparable affinity (11) (K_D, 58 nM) to the unmodified, HEK 293 cell-derived EphA3 exodomain (K_D, 86 nM). As expected, amino acid substitutions within the predicted Eph/ephrin dimerization and tetramerization interfaces resulted in reduction or loss of ephrin-A5 binding. Overall, mutations within the putative ephrin binding groove and directly exposed to ephrin (see Fig. 1) had the most severe effects, and in several cases (Table IV, $Thr^{102} \rightarrow Ala$, $Arg^{104} \rightarrow Gln$, $Gln^{150} \rightarrow Gly$, $Phe^{152} \rightarrow Leu$) their affinities were below the BIAcore measuring range (Fig. 2*a*). Interestingly, a change in side chain size at $Thr^{102} \rightarrow Gln$ affects ephrin binding some 150-fold less than the introduction of an aliphatic side chain ($Thr^{102} \rightarrow Ala$) at this position. In addition, mutations $Ser^{108} \rightarrow Gln$, $Ile^{109} \rightarrow Thr$, and $Leu^{111} \rightarrow Phe$ within the EphA3 G-H loop, forming the lid of the corresponding EphB2 ligand binding groove, greatly affected ephrin binding (Table IV).

Amino acid substitutions of residues within the H-I loop, previously shown as part of the "low affinity" tetramerization domain (17) ($Asp^{130} \rightarrow Gly$, $His^{131} \rightarrow Glu$, $Gly^{132} \rightarrow Glu$, and $Val^{133} \rightarrow Glu$), also impacted significantly on ephrin-A5 binding but less dramatically than the dimerization site mutants. By comparison, replacement of Gly^{132} and Val^{133}, residues immediately adjacent to the 4-residue alignment gap that is thought to determine Eph subclass specificity (17), had the most notable effects (Table IV).

Interestingly, replacement of $Asn^{208} \rightarrow Lys$, $Met^{218} \rightarrow Lys$, $Met^{218} \rightarrow Ile$, and $Asn^{233} \rightarrow Ile$, positioned in the cysteine-rich linker region outside the crystallographically characterized domain affected ligand binding significantly (3–5-fold, Table IV), but again to a lesser degree than mutations within the ligand binding groove.

Multivalent Ephrin-A5 Binding to Surface-tethered EphA3 Mutants—We next compared the binding of monovalent or divalent ephrins to sensor chip-tethered EphA3 mutants because divalent ephrin Fc derivatives, with the inherent capacity of docking to two distinct ligand binding interfaces simultaneously, are commonly used to study Eph function *in vivo*. w/t EphA3 ECD and mutants with substitutions either within the heterodimerization site (EphA3-$Phe^{152} \rightarrow Leu$) and the heterotetramerization site (EphA3-$Val^{133} \rightarrow Glu$) or mutated in both sites simultaneously (EphA3-Phe^{152},Val^{133}) were immobilized on parallel BIAcore sensor surfaces. In agreement with the results presented above, mutation of EphA3-Phe^{152} dramatically reduced ephrin-A5 binding (111-fold, Table V). By comparison, substitution of EphA3-Val^{133} affected ephrin-A5 binding only ~3-fold, and as a double mutant together with the Phe^{152} replacement, yielded a further 1.5-fold decrease of its binding affinity (Table V and Fig. 3*a*). Reduced binding affinity of mutant EphA3 seemed primarily due to increased dissociation rates, whereas a marginal effect on the association rate of the double mutant was noted. As expected, the binding of monovalent ephrin-B2, performed in a parallel control experiment, was below the BIAcore working range.

In agreement with previous studies (14) the interaction of divalent ephrin-A5 Fc revealed increased avidity (reduced off-rates), yielding an apparent affinity for w/t EphA3 of K_D of 0.1 nM. Binding of ephrin-A5 Fc, but not that of ephrin-B2 Fc analyzed in parallel, was increasingly perturbed by point mutants in the heterotetramerization and heterodimerization sites and mutation of both sites together (Table V and Fig. 3*b*). EphA3 ($Phe^{152} \rightarrow Leu$) showed a 56-fold reduced affinity (K_D, 5.6 nM), although the additional mutation at Val^{133} increased this effect only moderately (EphA3-Val^{133}, Phe^{152}, K_D, 7.4 nM). Interestingly, a nanomolar affinity maintained by the single and double mutants in this experimental setting suggests that residual ligand binding contacts of EphA3 contribute significantly to the overall interaction.

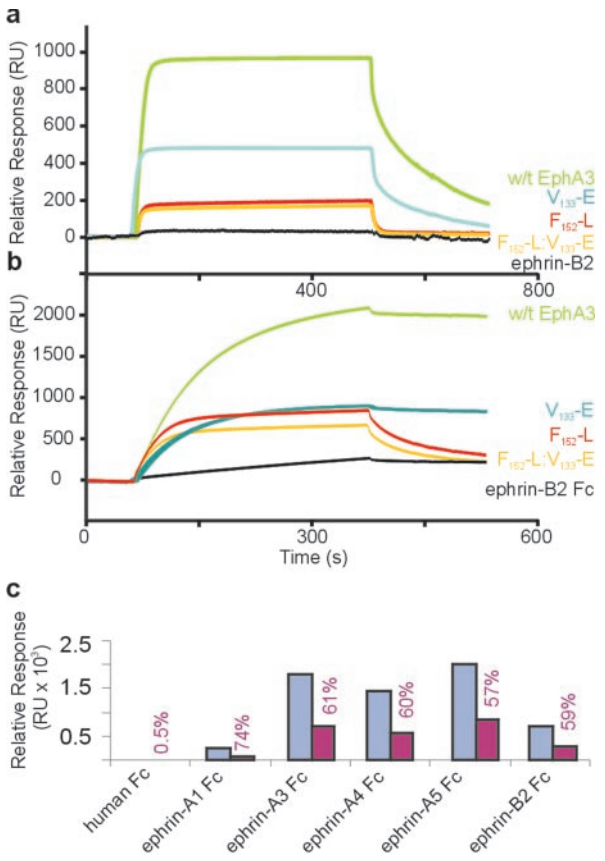

FIG. 3. **Effect of high and low affinity binding site mutations on ephrin binding characteristics of EphA3.** Parallel channels of BIAcore sensor chips were derivatized with either w/t EphA3, mutant EphA3$Val^{133} \rightarrow Glu$ (tetramerization site mutant), EphA3$Phe^{152} \rightarrow Leu$ (dimerization site mutant) or EphA3Phe^{152},Val^{133} (double mutant), and binding of monovalent ephrin-A5 (*a*) or divalent ephrin-A5 Fc (*b*) was monitored to determine kinetic parameters (Table V). Relative and corrected responses of 200 nM monovalent ephrin-A5 or 24 nM ephrin-A5 Fc binding are illustrated in the figures. *c*, comparison of the binding of various ephrin-Fc fusion proteins to w/t or $Val^{133} \rightarrow Glu$ mutant EphA3. Binding of ephrin-Fc fusion proteins, as indicated, or recombinant human Fc (25 nM) was analyzed on parallel channels of a BIAcore sensor chip derivatized with either the w/t (*light blue*) or mutant ($Val^{133} \rightarrow Glu$, *red*) EphA3 extracellular domain. The binding of human Fc domain at an equal concentration was used as a control in this experiment. The loss of binding due to the $Val^{133} \rightarrow Glu$ mutation is indicated (% of w/t response).

We also assessed the notion that mutation of EphA3 within the putative "specificity loop" (13) may affect the binding capacity of other EphA3-binding ephrins (14) differently to ephrin-A5 Fc. However, BIAcore responses of ephrin-A1 Fc, ephrin-A3 Fc, ephrin-A4 Fc, ephrin-A5 Fc, and ephrin-B2 Fc at equimolar (7.5 nM) concentrations were equally reduced (59–74%), suggesting that this single residue substitution has little effect on the suggested specificity-determining role (13) of this protein loop.

The IIIA4 mAb Binds to a Site Closely Adjacent but Not Overlapping the EphA3 Tetramerization Interface—Detailed binding analysis revealed that several EphA3 amino acid substitutions severely affected or abrogated binding of the IIIA4 mAb (Table IV). In particular mutants clustering within the tetramerization interface ($Asp^{130} \rightarrow Gly$, $Gly^{132} \rightarrow Glu$, and

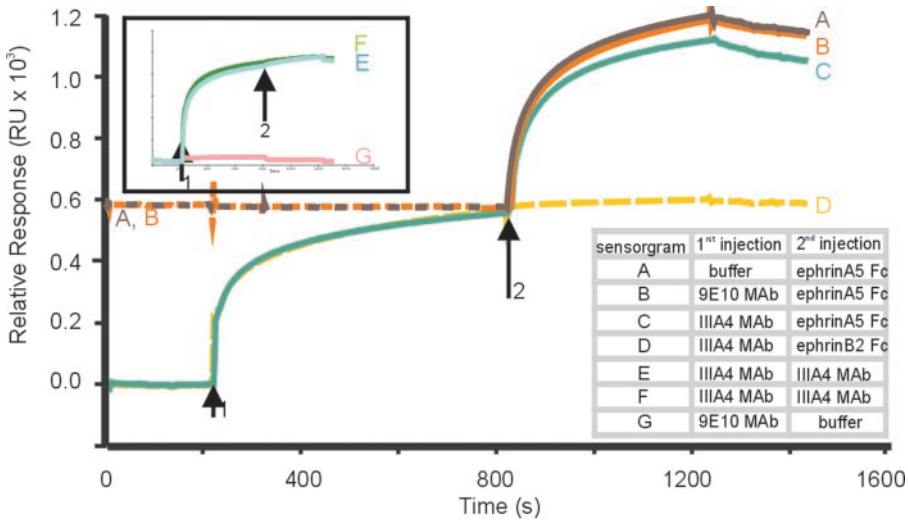

FIG. 4. **Consecutive binding of the IIIA4 α-EphA3 mAb and ephrin-A5 to SensorChip-tethered EphA3.** To test if ephrin-A5 and the IIIA4 mAb can bind simultaneously to EphA3, solutions (in BIAcore buffer) of IIIA4 (*C*, *D*, and *F*, 200 nM), anti-Myc 9E10 mAb used as control (*B* and *G*, 200 nM), or buffer (*A*) were injected onto an EphA3-derivatised sensor surface (indicated as ↑*1*). Following this injection of IIIA4 (or control antibody, 9E10) a subsequent injection (marked ↑*2*) of ephrin-A5 Fc (*A–C*, 25 nM) or a control protein (ephrin-B2 Fc, *D*) was introduced onto the same sensor surface. We confirmed in a control experiment that the first IIIA4 mAb injection (200 nM) indeed saturated the antibody binding capacity of the EphA3 sensor surface. To do this a second IIIA4 injection (*E* and *F*, 200 nM) was applied onto the sensor surfaces that had previously reacted with 100 nM (*E*) or 200 nM (*F*) IIIA4 mAb (*inset*). In the figure, the relative response levels of control samples *A* and *B* during the first injection cycle were adjusted to match the response level of the sensorgrams *C* and *D* in the second injection cycle.

Val^{133} → Glu) revealed significantly reduced IIIA4 binding, suggesting neighboring or overlapping binding sites of IIIA4 and of ephrin-A5. To address this, we examined whether saturation of IIIA4-binding sites would affect the binding of ephrinA5-Fc to an EphA3-coated sensor chip (Fig. 4). Comparing the binding of ephrin-A5 Fc to EphA3 sensor chip surfaces previously exposed to buffer (Fig. 4*A*) or IIIA4 (Fig. 4*C*) suggests a marginally reduced amount of bound ephrin-A5, due to a small apparent increase in the ephrin-A5 dissociation rate from IIIA4-loaded EphA3 (Fig. 4*C*). Exposure of the EphA3 surface with an isotype matched, non-relevant control antibody, tested in a parallel control experiment, did not change the binding characteristics of ephrin-A5 Fc (Fig. 4*B*). Interestingly, we could not detect an effect of IIIA4 binding on the interaction with monovalent ephrin-A5 (data not shown), suggesting that the dominating contribution from the high affinity binding site would mask detection of reduced binding at the low affinity binding site.

Both the Low and High Affinity Ephrin-binding Sites in EphA3 Are Essential for a Biological Response—To assess the functional relevance of selected ephrin-binding mutants, we tested their ability to trigger signaling of cell surface-expressed EphA3. To monitor ephrin-A5 binding to HEK 293 cell surface-expressed w/t and mutant EphA3, we introduced the single residue, Phe^{152} → Leu, and the double residue, Val^{133} → Glu, Phe^{152} → Leu mutation into full-length EphA3 containing a C-terminal GFP (green fluorescence). Transfection of HEK 293 cells with corresponding expression constructs revealed abundant cell membrane as well as cytoplasmic expression of the GFP-tagged receptor constructs (*green fluorescence*, Fig. 5*a*). To monitor ligand binding, we attached Alexa 546 to ephrin-A5 Fc (*red fluorescence*). Results summarized in Fig. 5 confirm avid Alexa 546-ephrin-A5 Fc binding to w/t EphA3, or to the 3xYF EphA3 mutant, lacking juxtamembrane and activation loop tyrosines (5) and used as control (see below). Merged images of *green* and *red* fluorescent micrographs indicate prominent areas of the fluorescent proteins at the cell membrane (merged yellow image), as well as co-localized cytoplasmic patches (*yellow*) of ephrin-A5 Fc (*red*) and EphA3 (*green*) fluorescence, suggesting internalization of GFP-EphA3/Alexa 546-ephrin-A5 Fc complexes. In agreement with the findings from kinetic experiments, cells expressing EphA3-Phe^{152} → Leu as well as EphA3-Phe^{152},Val^{133} expressing cells, reveal greatly reduced, ephrin-A5 Fc binding.

We next studied the effect of ephrin-A5 binding mutations on EphA3 signaling by immunoprecipitation analysis of w/t or mutant EphA3-transfected HEK 293 cell lysates, using EphA3 phosphorylation and CrkII recruitment as essential criteria for EphA3-directed cellular responses (5). Mutations within the dimerization (Phe^{152} → Leu) and tetramerization (Val^{133} → Glu) domains reduced ephrin-A5-mediated trans-phosphorylation and CrkII recruitment (Fig. 5*f*) to levels below those recorded with signaling-deficient 3xYF EphA3, lacking the essential autophosphorylation sites (5). Importantly, the Asn^{232} → Ile mutation within the cysteine-rich hinge region also results in marginal EphA3 phosphorylation and CrkII recruitment, emphasizing the functional importance of this newly identified binding interface.

Together our experiments indicate that although EphA3 mutants with single residue substitutions in the heterodimerization or tetramerization sites, or in the cysteine-rich hinge region, all maintain residual ephrin-A5 binding capacity, an Eph-ephrin complex with all three sites intact is essential for EphA3 activation and downstream signaling.

DISCUSSION

A Novel Mutagenesis Approach for Structure/Function Analysis—We describe a novel mutagenesis strategy that allowed us to identify Eph receptor surfaces that are essential for ephrin binding and the initiation of Eph receptor signaling. Our approach is based on isolation of ephrin binding-compromised proteins from a library of random EphA3 point mutants that cover receptor domains implicated in ephrin binding and the initiation of biological responses (10, 11). Analyzing secreted mutant proteins during the primary colony screen, both functionally (for compromised ephrin-A5 binding) and immunologically (for native conformation), allowed an immediate and efficient selection of receptor mutants (7%) with altered ligand interaction sites and exclusion of those with a more global disruption of their overall domain structure. Effective

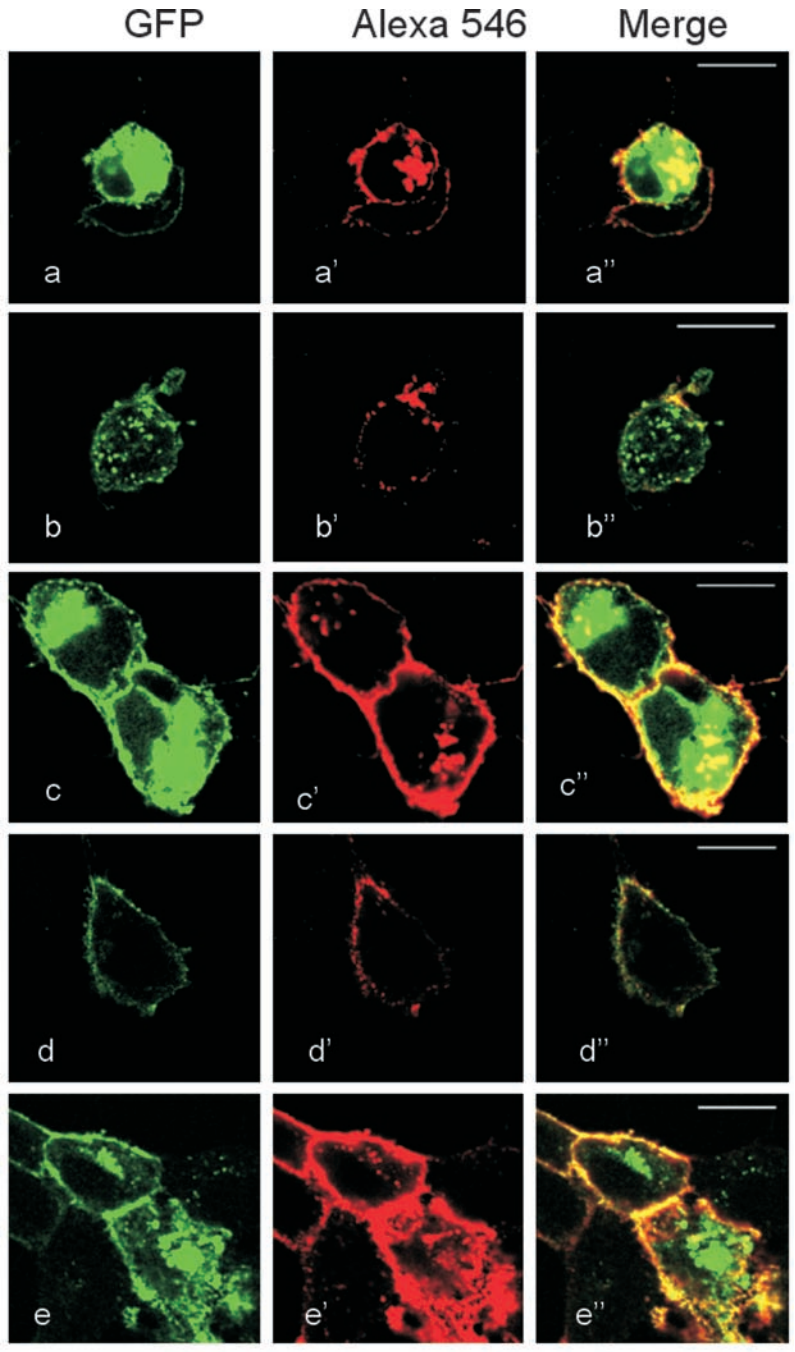

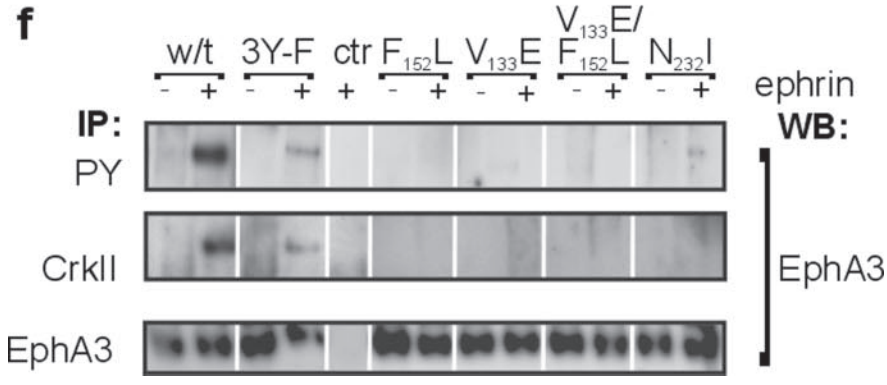

FIG. 5. **Val^{133} → Glu and Phe^{152} → Leu mutations affect ephrin-A5 binding, receptor phosphorylation, and CrkII recruitment in EphA3 expressing HEK 293T cells.** HEK 293T cells transiently transfected with chimeric proteins of GFP fused to the C terminus of non-mutated EphA3 (*a*), EphA3-Phe^{152} → Leu (*b*), EphA3Val^{133} → Glu (*c*), EphA3Val^{133}/Phe^{152} (*d*), or EphA3-Tyr^{596,602,779} → Phe (5) (*e*) used as control were exposed (10 min) to Alexa-labeled ephrin-A5 Fc, and non-bound ephrin-A5 Fc was removed by washing (phosphate-buffered saline) prior to fixation and microscopy. Images of GFP fluorescence (*green, a–e*), Alexa 546 fluorescence (*red, a′–e′*), and merged images (*yellow, a″–e″*) of GFP and Alexa 546 fluorescence are shown. Fluorescence signals inside the cells represent cytosolic pools of GFP-EphA3 (*green*) as well as internalized Alexa-labeled ephrin-A5 Fc (*red*) complexed to GFP-EphA3. *f*, anti-phosphotyrosine and anti-Crk immunoprecipitates from Triton X-100 lysates of HEK 293 cells transfected with w/t or mutant EphA3 or with a vector control (as indicated) were stimulated with pre-clustered ephrinA5-Fc and analyzed by Western blot (*WB*) with anti-EphA3 antibodies. To assess even loading, parallel samples from the same lysates were immunoprecipitated (*IP*) with IIIA4 anti-EphA3. In parallel control samples, immunoblot analysis was performed with cells expressing EphA3-Tyr^{596,602,779} → Phe, mutated at the principle auto-phosphorylation sites and yielding marginal levels of EphA3 phosphorylation and CrkII recruitment (5).

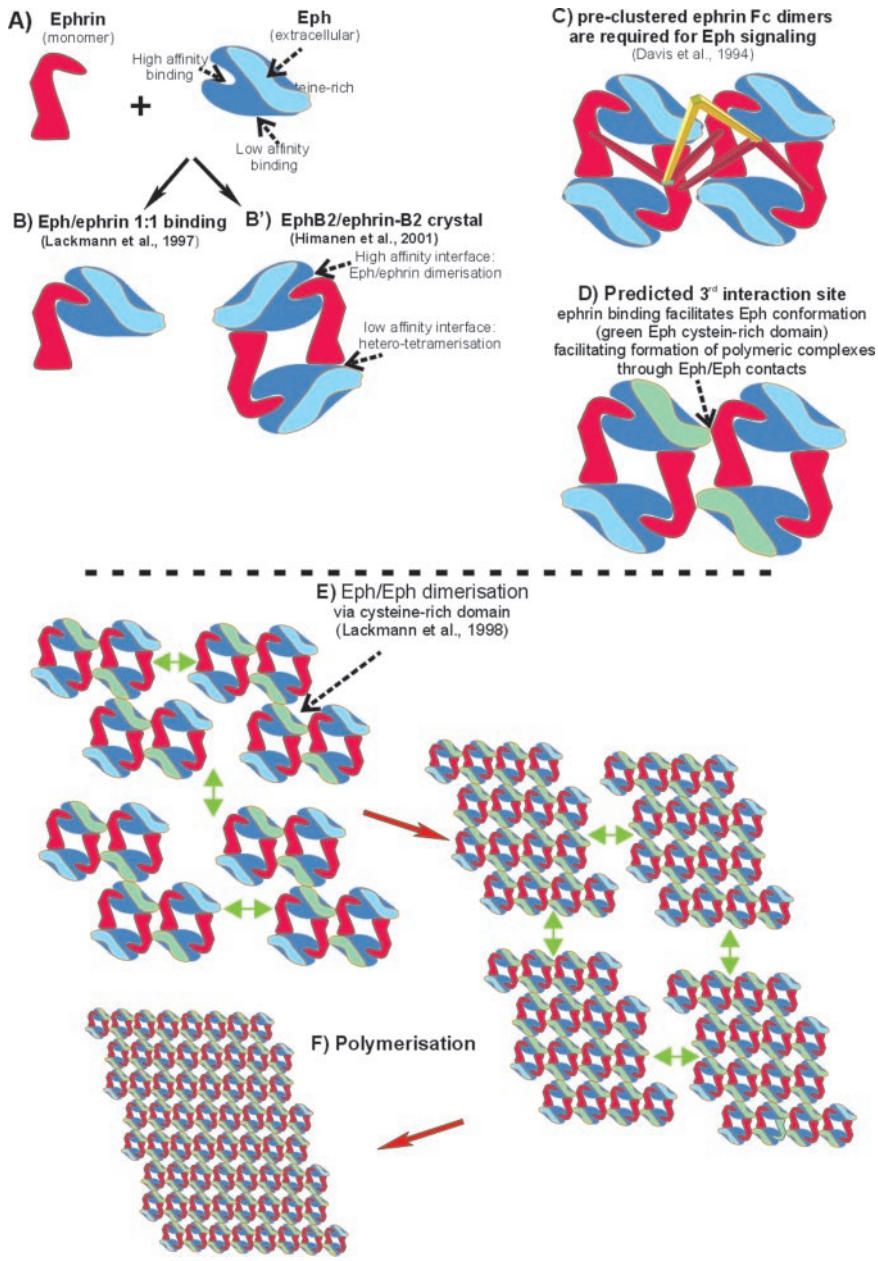

FIG. 6. **Model of ephrin-induced Eph clustering.** Monomeric Ephs and ephrins (*A*) combine into dimeric or tetrameric complexes; high affinity Eph/ephrin dimers (14) (*B*) assemble via a lower affinity interface into Eph/ephrin heterotetramers (17) (*B′*). Functional studies (15) demonstrated a requirement for cross-linking (via anti-Fc antibodies, *yellow fork*) of dimeric ephrins-Fc fusion proteins (*red*) to trigger Eph signaling and biological responses (*C*). *In vivo*, membrane-bound ephrin can engage in additional Eph contacts to facilitate the formation of higher order Eph/ephrin signaling clusters. A candidate interface for these contacts is the third binding site between ligand binding and cysteine-rich domains, now identified in our mutagenesis study (*D*). We hypothesize that ligation at this interface (↔) triggers the formation of Eph/Eph contacts through the cysteine-rich domain (↕), an interaction that has documented importance for Eph signaling (11) (*E*). These low affinity interactions are notable *in vitro* only with pre-clustered ephrins and *in vivo* would require a critical ephrin density on the cell membrane. We postulate that the cluster of Eph/ephrin tetramers is sufficient as nucleus for "cluster polymerization" (*F*). The final size of the cluster thus would depend on the local Eph and ephrin density.

isolation of mutants with intact global protein architecture was facilitated largely by selecting mutant proteins through their capacity of binding IIIA4, a mAb previously used successfully to monitor the biological integrity of recombinant EphA3 (21). Sequencing of 84% (38/45) of the clones recovered from this screen revealed, either by alignment to known EphB2/ephrin-B2 interaction surfaces or by functional assay, that in 37/38 cases at least one of the mutated amino acids is either directly involved with or falls within the immediate vicinity of predicted Eph/ephrin contacts (Table III). It is of note that in double mutant yeast colonies, loss of ephrin binding was generally due to one severe mutation within and a less disruptive mutation on the margin or outside a high affinity binding domain (Table IV). Overall, the integration of library screen and detailed kinetic analysis allowed us to accurately pinpoint essential ephrin contact points on the EphA3 ECD. Although previous structure/function studies (10, 11) and crystallography (18) already offered important insights into the molecular architecture of Eph-ephrin complexes, the receptor mutants described here provide the first available reagents to test the predictions drawn from these studies. We believe that the success of this strategy to reliably identify protein/protein interaction surfaces suggests its general applicability for the study of other receptor/ligand systems.

Functional Mutant Analysis Defines Three Distinct Ephrin Interaction Surfaces—Bi-directional Eph/ephrin signaling between opposing cells is facilitated by multimeric receptor-ligand complexes, and elucidation of the EphB2/ephrin-B2 crystal structure (17) allowed detailed predictions of the protein interfaces that are essential for the formation of an active signaling complex (18). The proposed heterotetrameric ring-like model structure, held together by two distinct (low and high surface area) contact surfaces that position the Eph and ephrin C termini to opposite sites of the crystal plane, provides a structural basis for the requirement of higher order Eph-ephrin complexes to initiate bi-directional signals. However, to date there was no functional data to confirm the requirement of two distinct Eph/ephrin contact sites for Eph/ephrin signaling.

We now provide, for the first time, evidence for the functional relevance of these two distinct interfaces, both for high affinity ephrin binding and for the initiation of Eph downstream sig-

naling. Alignment of the isolated mutants onto a putative EphA3/ephrin-A5 structure (Fig. 1) confirms two clusters positioned within or in the immediate vicinity of the extensive dimerization domain and the smaller tetramerization interface.

A first group of mutant residues that cluster within or around the proposed ephrin binding groove of the dimerization domain ($Glu^{41} \rightarrow Arg$, $His^{50} \rightarrow Gln$, $Glu^{53} \rightarrow Lys$, $Val^{58} \rightarrow Ala$, $Thr^{102} \rightarrow Ala$, $Arg^{104} \rightarrow Glu$, $Ser^{108} \rightarrow Gly$, $Ile^{109} \rightarrow Thr$, and $Phe^{152} \rightarrow Leu$, Tables III and IV), and which are involved in Van der Waals and intermolecular hydrogen bonds in the corresponding EphB2-ephrin-B2 complex, essentially ablate binding of monovalent ephrin. Thus, single amino acid substitutions within the high affinity binding region of EphA3 (Table IV) reduce binding to ephrin-A5 surfaces to background levels, suggesting that other ephrin binding interfaces on their own are insufficient to mediate effective one-to-one contacts. Interestingly, we observe marginal binding of monovalent but significant binding of divalent ephrin-A5 Fc to a mutant EphA3-$Phe^{152} \rightarrow Leu$ sensor surface (Table V), the latter representing practically a "high density array" of different ephrin interaction sites. Although differences in accessibility of interaction sites of immobilized ephrin-A5 or EphA3 could account for this contrasting kinetic behavior, increased avidity of divalent ephrin-A5 Fc, in particular to bind to several possible sites on this "array," may also contribute to increased binding. It is of note in this context that, inherent to our BIAcore analysis, kinetic properties are derived from the interacting behavior of associated components *in situ* rather than from their condition at thermodynamic equilibrium.

A second cluster of mutants, mapping to the proposed tetramerization site of the model structure, reveals affinity changes that are orders of magnitude smaller than those of mutations within the high affinity groove. The quantitation of "mutant severity" by kinetic binding analysis seems to correlate with the contribution of corresponding w/t residues to the structural stability of the predicted complex. In this latter case, significant binding of (tetramerization site) mutant receptor to sensor surface-tethered ephrin (Table IV) suggests a dominating contribution of the high affinity dimerization interface to the overall interaction. Importantly, placement of representative mutants from either the dimerization or the tetramerization interface into cell surface-expressed, full-length EphA3 dramatically reduces trans-phosphorylation and initiation of downstream signaling (Fig. 5*f*), demonstrating the requirement of both interactions for an active signaling complex.

Finally, and most importantly, a distinct group of mutants identified in our screen, including $Asn^{208} \rightarrow Lys$, $Leu^{209} \rightarrow Gln$, $Met^{218} \rightarrow Lys$, $Val^{231} \rightarrow Asp$, $Asn^{232} \rightarrow Ile$, and $Ser^{245} \rightarrow Arg$, delineate a novel Eph/ephrin interaction interface within the cysteine-rich hinge region that has not been characterized within the EphB2/ephrin-B2 crystal structure. These mutants cluster within two short sequence motifs Asn^{208} to Ala^{210} and Val^{231} to Ser^{235} that are conserved in human, mouse, chicken, and zebrafish EphA3, EphA4, and EphA5 but not in other Eph proteins. It is of note that these three Eph receptors share a highly conserved and well described ephrin-A5-dependent, axon guidance function during development of the visual system (3). While overall, the ephrin binding capacity of these mutants is less affected than that of the previously described ones, marginal signaling in $Val^{231} \rightarrow Asp$ EphA3 clearly emphasizes the importance of this interface for the formation of biologically active EphA-ephrin complexes.

Proposed Mechanisms That Assemble Active Eph-Ephrin Signaling Complexes—By taking the findings from the current study and from the molecular architecture of the EphB2-ephrin-B2 complex (18) into consideration, we suggest that ephrin-induced EphA3 clustering into active signaling complexes involves at least three distinct binding interfaces (Fig. 6). A 1:1 interaction of monovalent, soluble ephrin with EphA3 is facilitated primarily through docking to the high affinity binding groove, whereas binding of soluble, monovalent ligand to the low affinity domains (*i.e.* as the predicted residual ephrin-A5 binding to a high affinity binding site mutant) is not detected in our experiments. The two binding interfaces within the crystallized ephrin-binding domain are positioned in a manner that a single ephrin cannot engage in both sites simultaneously, a feature that emphasizes the necessity of dimeric (*e.g.* Fc-tethered) or multimeric ligands to enable the assembly of Ephs into tetrameric, or possibly higher order, signaling complexes (18). Experimental evidence further demonstrates that clustering of Fc-tethered ligands is essential for activation of downstream signaling and biological responses, thus implying the formation of higher order clusters (15). The third ephrin interaction site outside the globular ligand-binding domain is a likely candidate for the Eph structure that participates in this clustering mechanism. The position of this interface as linker between the previously defined ephrin binding (17) and Eph-Eph dimerization domains (11) invokes the intriguing possibility that ephrin docking to this site induces an orientation of receptors that leads to aggregation into larger Eph/ephrin signaling clusters (Fig. 6*E*). In line with this hypothesis, previous studies indicated that EphA3/EphA3 contacts via the EGF-like domain can facilitate Eph phosphorylation and are essential for receptor function (11). In ongoing experiments we are now using the Eph receptor mutants discussed in this study to examine the mechanisms of ephrin-independent EphA3 dimerization.

REFERENCES

1. Lemke, G. (1997) *Mol. Cell. Neurosci.* **9,** 331–332
2. Boyd, A. W., and Lackmann, M. (2001) *Science's STKE* http:/www.stke.org/cgi/content/full/OC_sigtrans;2001/RE20
3. Wilkinson, D. G. (2001) *Nat. Rev. Neurosci.* **2,** 155–164
4. Dodelet, V. C., and Pasquale, E. B. (2000) *Oncogene* **19,** 5614–5619
5. Lawrenson, I. D., Wimmer-Kleikamp, S. H., Lock, P., Schoenwaelder, S. M., Down, M., Boyd, A. W., Alewood, P. F., and Lackmann, M. (2002) *J. Cell Sci.* **115,** 1059–1072
6. Hattori, M., Osterfield, M., and Flanagan, J. G. (2000) *Science* **289,** 1360–1365
7. Kullander, K., and Klein, R. (2002) *Nat. Rev. Mol. Cell Biol.* **3,** 475–486
8. Holmberg, J., and Frisen, J. (2002) *Trends Neurosci.* **25,** 239–243
9. Drescher, U. (2002) *Curr. Opin. Genet. Dev.* **12,** 397–402
10. Labrador, J. P., Brambilla, R., and Klein, R. (1997) *EMBO J.* **16,** 3889–3897
11. Lackmann, M., Oates, A. C., Dottori, M., Smith, F. M., Do, C., Power, M., Kravets, L., and Boyd, A. W. (1998) *J. Biol. Chem.* **273,** 20228–20237
12. Wicks, I. P., Wilkinson, D., Salvaris, E., and Boyd, A. W. (1992) *Proc. Natl. Acad. Sci. U. S. A.* **89,** 1611–1615
13. Himanen, J. P., Henkemeyer, M., and Nikolov, D. B. (1998) *Nature* **396,** 486–491
14. Lackmann, M., Mann, R. J., Kravets, L., Smith, F. M., Bucci, T. A., Maxwell, K. F., Howlett, G. J., Olsson, J. E., Vanden Bos, T., Cerretti, D. P., and Boyd, A. W. (1997) *J. Biol. Chem.* **272,** 16521–16530
15. Davis, S., Gale, N. W., Aldrich, T. H., Maisonpierre, P. C., Lhotak, V., Pawson, T., Goldfarb, M., and Yancopoulos, G. D. (1994) *Science* **266,** 816–819
16. Stein, E., Lane, A. A., Cerretti, D. P., Schoecklmann, H. O., Schroff, A. D., Van Etten, R. L., and Daniel, T. O. (1998) *Genes Dev.* **12,** 667–678
17. Himanen, J. P., Rajashankar, K. R., Lackmann, M., Cowan, C. A., Henkemeyer, M., and Nikolov, D. B. (2001) *Nature* **414,** 933–938
18. Himanen, J. P., and Nikolov, D. B. (2003) *Trends Neurosci.* **26,** 46–51
19. Coulthard, M. G., Lickliter, J. D., Subanesan, N., Chen, K., Webb, G. C., Lowry, A. J., Koblar, S., Bottema, C. D., and Boyd, A. W. (2001) *Growth Factors* **18,** 303–317
20. Jenkins, B. J., D'Andrea, R., and Gonda, T. J. (1995) *EMBO J.* **14,** 4276–4287
21. Lackmann, M., Bucci, T., Mann, R. J., Kravets, L. A., Viney, E., Smith, F., Moritz, R. L., Carter, W., Simpson, R. J., Nicola, N. A., Mackwell, K., Nice, E. C., Wilks, A. F., and Boyd, A. W. (1996) *Proc. Natl. Acad. Sci. U. S. A.* **93,** 2523–2527
22. Sali, A., and Blundell, T. L. (1993) *J. Mol. Biol.* **234,** 779–815
23. Smith, D. K., and Treutlein, H. R. (1998) *Protein Sci.* **7,** 886–896
24. Hinds, M. G., Lackmann, M., Skea, G. L., Harrison, P. J., Huang, D. C., and Day, C. L. (2003) *EMBO J.* **22,** 1497–1507

Dissecting the EphA3/Ephrin-A5 Interactions Using a Novel Functional Mutagenesis Screen

Fiona M. Smith, Christopher Vearing, Martin Lackmann, Herbert Treutlein, Juha Himanen, Ke Chen, Allan Saul, Dimitar Nikolov and Andrew W. Boyd

J. Biol. Chem. 2004, 279:9522-9531.
doi: 10.1074/jbc.M309326200 originally published online December 2, 2003
